Crystallization-Controlled Limitations of Melt Spinning

Andrzej Ziabicki, Leszek Jarecki

Institute of Fundamental Technological Research, Polish Academy of Sciences, Świętokrzyska 21, 00-049 Warsaw, Poland

Received 9 March 2006; accepted 11 July 2006
DOI 10.1002/app.26121
Published online in Wiley InterScience (www.interscience.wiley.com).

ABSTRACT: A numerical simulation of melt spinning reveals bifurcation of dynamic solutions leading to limited spinning conditions. The bifurcation phenomenon is controlled by stress-oriented crystallization and crystallinity-dependent polymer viscosity. Under the conditions of bifurcation, the space of the spinning conditions (take-up velocity × filament thickness) splits into three regions corresponding to amorphous fibers, partially crystalline fibers, and inaccessible conditions. Major factors affecting the maximum spinning speed and minimum filament thickness for melt-spun poly(ethylene terephthalate) are analyzed. © 2007 Wiley Periodicals, Inc. J Appl Polym Sci 105: 215–223, 2007

Key words: crosslinking; crystallization; simulations; stress; viscosity

INTRODUCTION

Current trends in melt-spinning technology involve an increase in the production rates and a reduction of the filament thickness. The conditions under which fibers can be produced are not unlimited, however. The available spinning speed and filament thickness strongly depend on the material properties and spinning conditions.

A natural limitation of the spinning speed and filament thickness is the unstable deformation of the polymer melt. In addition to such effects as the heterogeneity of the melt and the variation of the extrusion rate, take-up speed, and cooling conditions, an important role is played by the rheological properties of the polymer. Irregular flow at the spinneret exit (melt fracture and capillary breakup) may lead to disintegration of the polymer jet, making continuous formation of smooth filaments impossible.[1] The hydrodynamic instability of viscous[2–5] and viscoelastic[6–8] polymer melts may lead to draw resonance and the formation of irregular fibers.

This article is concerned with another source of limitations. The maximum spinning speed and minimum filament thickness may be controlled by stress-induced crystallization, leading to many-valued solutions of the dynamic equations of melt spinning.[9–12] In a steady-state process, the same boundary conditions may correspond to two or more stress profiles and different structures of the resulting fibers. The physical mechanism of this phenomenon is analyzed in ref. 12. In this article, the effects of the material properties of crystallizable polymers on the accessible range of spinning conditions are discussed, and ways are suggested to modify the spinning process.

MATHEMATICAL MODEL OF MELT SPINNING: GOVERNING EQUATIONS AND BOUNDARY CONDITIONS

Figure 1 presents a scheme for single-filament melt spinning. The polymer melt is extruded at a constant temperature, T_0, through an orifice with diameter d_0, at a constant mass flow rate, W, which determines the constant extrusion velocity, V_0. The polymer jet is elongated in direction z and collected at the distance of $z = L$ with a constant take-up velocity, V_L, which determines the constant filament thickness (titer), T_d. Cooling of the melt is controlled by a horizontal stream of air (40 m/s) with a constant temperature, T_∞.

We will discuss the effects of crystallization, using the simplified model of melt spinning developed in our laboratory.[9–12] The model is based on a thin filament approximation neglecting the radial distribution of kinematic and dynamic characteristics (velocity V, temperature T, and axial tension F). Instead of radially differentiated variables [$V(z,r)$, $T(z,r)$, etc.], average variables integrated over a filament cross section [$\overline{V}(z)$, $\overline{T}(z)$, ...] are used. This reduces the dynamic equations to one dimension—coordinate z—measured along the spin line from the spinneret to the winding device.

The steady-state mass conservation equation assumes the following form:

$$\overline{\rho}(z)R^2(z)\overline{V}(z) = W \tag{1}$$

This article is dedicated to the memory of Professor Marian Kryszewski.

Correspondence to: A. Ziabicki (aziab@ippt.gov.pl).

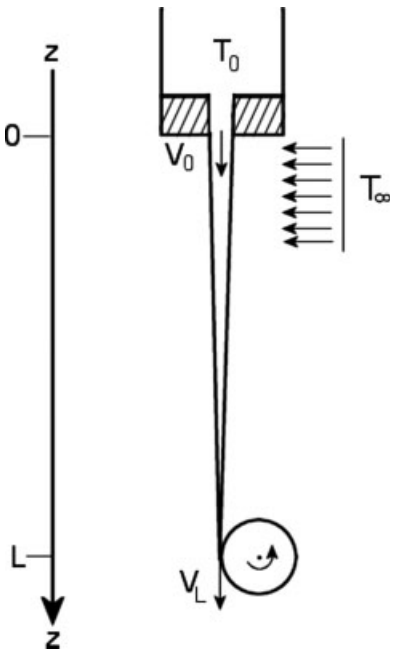

Figure 1 Scheme of regular melt spinning.

where W is the mass flow intensity, ρ is the average density, R is the radius of the filament at distance z from the extrusion point, and $\overline{V}$ is the average axial velocity.

In this article, two other conservation equations in the original model[9–11] have been simplified.

In the equation of motion, the effects of gravity, surface tension, and air drag have been neglected, leaving only a convective inertial term:

$$\frac{dF}{dz} = W\,\overline{V}\frac{d\overline{V}}{dz} \tag{2}$$

where $F(z)$ is the local tension (axial force) at distance z from the extrusion point. The justification for neglecting air friction results from the fact that deformation and oriented crystallization are concentrated in the zone close to the spinneret, where air friction is rather small and tension is dominated by inertia.

In the energy conservation equation, the heat of crystallization and viscous dissipation have been neglected, leaving only convective heat transfer from the surface of the filament to the cooling medium. The axial gradient of the average temperature reduces to

$$\frac{d\overline{T}}{dz} = -\frac{2\alpha^*}{\overline{\rho}C_pR\overline{V}}(\overline{T} - T_\infty) = -\frac{2\pi R\alpha^*}{C_pW}(\overline{T} - T_\infty) \tag{3}$$

where C_p denotes the specific heat of the filament, α^* is the surface coefficient of heat transfer, and T_∞ is the constant temperature of the cooling medium. From ref. 13, we have

$$R\alpha^* = 0.42\,\lambda_s\left(\frac{4W\overline{V}}{\pi\nu_s^2\overline{\rho}}\right)^{1/6} \tag{4}$$

where λ_s and ν_s denote the thermal conductivity and kinematic viscosity of the cooling medium (air), respectively. Equations (3) and (4) reduce to

$$\frac{d\ln(\overline{T} - T_\infty)}{dz} = \frac{-0.84\,\lambda_s}{C_pW}\left(\frac{4W\overline{V}}{\pi\nu_s^2\overline{\rho}}\right)^{1/6} \tag{5}$$

Conservation equations have to be combined with constitutive and structure evolution equations. For the sake of simplicity, the linear constitutive model is used: an incompressible Newtonian fluid with a position-dependent viscosity [$\eta(z)$]. The local temperature gradient affects the viscosity much more strongly than the elongation rate. Viscoelastic effects, which may contribute to filament breaks or deformation instability, are not considered.

Stress tensor $\mathbf{p}$, averaged over the filament cross section, reduces to a diagonal form, and the normal stress difference, $\Delta\overline{p}$, can be expressed through axial tension F:

$$\begin{aligned}\mathbf{p} + p_0\mathbf{I} &= 2\eta\,(z)\,\dot{\mathbf{e}} = \eta\cdot(\nabla V + \nabla V^T)\\ \Delta\overline{p} &= \frac{F(z)}{\pi R^2(z)} = 3\eta\,(z)\frac{d\overline{V}}{dz}\end{aligned} \tag{6}$$

The local shear viscosity, $\eta(z)$, depends on the local temperature and local degree of crystallinity (volume fraction of the crystalline phase):

$$\eta(z) = \eta_T[\overline{T}(z)]\cdot\eta_X[\overline{X}(z)] \tag{7}$$

where η_T, and η_X describe temperature and crystallinity effects.

The temperature factor, η_T, can be described with a variety of empirical formulas. In this work, an Arrhenius formula with a constant activation energy, E, is used:

$$\eta_T(\overline{T}) = \eta_0\,e^{E/k\overline{T}} \tag{8}$$

where η_0 is a melt viscosity parameter and k is Boltzmann constant. For poly(ethylene terephthalate) (PET) melts, the following formula has been used:[14,15]

$$\eta(T, M_\eta) = 2.769\times10^{-19}\,M_\eta^{3.427}\exp\left[\frac{6923.7}{T}\right] \tag{9}$$

where M_η is the viscosity-average molecular weight.

Different empirical formulas have been used to describe the dependence of the melt viscosity on the

crystallinity.[16–24] What we are using is the hyperbolic function

$$\eta_X(X) = \begin{cases} 1 & \text{for } X = 0 \\ \dfrac{X_{\mathrm{cr}}}{X_{\mathrm{cr}} - X} & \text{for } 0 < X < X_{\mathrm{cr}} \\ \infty & \text{for } X \geq X_{\mathrm{cr}} \end{cases} \tag{10}$$

based on the model in which crystallites, acting as physical crosslinks, cause the aggregation of macromolecules and ultimately convert the fluid melt into a solid, elastic network.[16,22] A formula, similar to eq. (10), has also been used for concentrated suspensions[17] and polymer melts.[24] The critical degree of crystallinity, X_{cr}, corresponds to the gelation point at which the viscosity is infinite and no flow is possible. In our simulations, $X_{\mathrm{cr}} = 0.1$ has been assumed.

The assumption of crystallinity-dependent viscosity makes it necessary to complete the system of governing equations with a crystallinity evolution equation. The crystallization kinetics are described by the nonisothermal, quasi-static form[25,26] of the Kolmogoroff–Avrami–Evans equation:

$$\begin{aligned} &\frac{d\ln(1-X)}{dt} = -\frac{dE}{dt} \\ &\frac{dE}{dt} = n\left[\int_0^t \frac{K(t')}{\overline{V}}\,dt'\right]^{n-1} K(t) = n\,E^{n-1/n}\,K(t) \\ &K(t) = K[\overline{T}(t), \Delta\overline{p}(t)] \end{aligned} \tag{11}$$

Crystallization rate characteristic K is controlled by the average temperature, $\overline{T}$, and average normal stress difference, $\Delta\overline{p}$. The following empirical formula is used:[1]

$$K(\overline{T},\Delta\overline{p}) = \begin{cases} 0 & \text{for } \overline{T} > T_m \\ K_0 \exp\left[\frac{-4\ln 2(\overline{T}-T_{\max})^2}{D^2}\right] \cdot \exp\left[A\left(\frac{\Delta\overline{p}}{\Delta p_i}\right)^2\right] & \text{for } T_g \leq \overline{T} \leq T_m \\ 0 & \text{for } \overline{T} < T_g \end{cases} \tag{12}$$

where A is a stress-induced crystallization parameter, K_0 is the maximum thermal crystallization rate, and $T_{\max}$ is the maximum thermal crystallization rate temperature. The reference stress, Δp_i, is related to optical birefringence of ideally oriented fibers, Δn_i.

$$\frac{\Delta p}{\Delta p_i} = \frac{\Delta n}{\Delta n_i} = f \tag{13}$$

For PET, Δp_i is 2.82×10^7 Pa.[27,28] The normal stress or optical birefringence ratio ($\Delta n/\Delta n_i$) is equal to the molecular orientation factor, f.

Four first-order differential equations for average velocity $\overline{V}(z)$, tension $F(z)$, temperature $\overline{T}(z)$, and crystallinity $\overline{X}(z)$ require four boundary conditions. At the extrusion point:

$$\begin{aligned} &\overline{V}(z=0) = V_0 \\ &F(z=0) = F_0 \\ &\overline{T}(z=0) = T_0 \\ &\overline{X}(z=0) = 0 \end{aligned} \tag{14}$$

In contrast to V_0, T_0, and X_0, the initial tension, F_0, is not defined *a priori*. On the other hand, the process of spinning imposes another constraint on the velocity at $z = L$. To obtain unknown value F_0 as a function of the known value of V_L, an inverse problem is solved. Values of F_0 are assumed, and the corresponding V_L values are calculated. The set of boundary conditions reduces to

$$\begin{aligned} &\overline{V}(z=0) = V_0 \\ &\overline{V}(z=L) = V_L \Rightarrow F_0 \\ &\overline{T}(z=0) = T_0 \\ &\overline{X}(z=0) = 0 \end{aligned} \tag{15}$$

NUMERICAL SIMULATION OF MELT SPINNING PET FIBERS

PET provides a good example of a crystallizable, fiber-forming polymer. In addition to being an important source of textile and industrial fibers, PET can be obtained in a wide range of structures ranging from glassy–amorphous structures to highly crystalline ones. The crystallization rates, sensitive to the temperature and stress, may be controlled by the variation of the spinning conditions. A standard set of material characteristics used for the simulation is given in Table I.

There are two different spinning regimes in which the effects of spinning velocity can be compared: a constant mass throughput and a constant filament thickness (titer). The first is often used in laboratory studies, and the latter is typical for industrial spinning.

Figure 2 presents the relationship between take-up velocity V_L and initial force F_0 at constant W. An increase in V_L reduces the filament thickness (titer, T_d) and increases the cooling rate and viscosity gradient:

$$\begin{aligned} &W = 1/4\,\rho\pi d_L^2 V_L \\ &W = \text{const} \Rightarrow Td \propto \frac{1}{V_L} \\ &\left|\frac{-d\ln(\overline{T}-T_\infty)}{dz}\right| \propto \overline{V}^{1/6} \\ &\frac{d\eta}{dz} = \frac{\partial\eta}{\partial\overline{T}}\,\frac{d\overline{T}}{dz} \propto \frac{\overline{V}^{1/6}}{\overline{T}-T_\infty} \end{aligned} \tag{16}$$

TABLE I
Standard Set of Material Characteristics for the Simulation of PET Spinning

Parameter	Value	Reference
Melting temperature (T_m; K)	553	47
Glass-transition temperature (T_g; K)	340	47
Maximum thermal crystallization rate temperature (T_{max}; K)	463	1
Maximum thermal crystallization rate (K_0; s^{-1})	0.016	1
Half-width of the crystallization rate (D; K)	32	1
Stress-induced crystallization parameter (A)	500	29
Reference stress (Δp_i; Pa)	2.82×10^7	27, 28
Viscosity-average molecular weight (M_η; Da)	32,000	
Activation energy for viscous flow (E/k; K)	6923.7	14
Melt viscosity parameter (η_0; kPa s)	0.7612	14
Critical crystallinity for gelation (X_{cr})	0.1	30

In the range of small and moderate velocities, $V_L(F_0)$ is a monotonically increasing function. The increase in F_0 is a result of a simultaneous increase in the deformation rate and viscosity. In the absence of crystallization, monotonic $V_L(F_0)$ behavior would extend over the entire range of spinning conditions.

In crystallizable polymers, such as PET, V_L exhibits a minimum value ($V_L = V_{L,bif}$) and a maximum value ($V_L = V_{L,max}$). In the point of the minimum, bifurcation of dynamic solutions can be observed. Two or more different solutions (different F_0 values) satisfy the same system of governing equations and the same boundary conditions (V_L). It has been shown in our earlier simulations that the left-hand branch of the $V_L(F_0)$ function (dashed line) corresponds to amorphous fibers, and the right-hand one (solid line) corresponds to partially crystalline fibers.[9–11] Thus, the appearance of bifurcation is associated with the onset of crystallization, and a sharp peak at which both branches merge ($V_L = V_{L,max}$, presents a maximum take-up velocity. No fibers can be spun at take-up speeds higher than $V_{L,max}$.

The other spinning regime is the constant filament thickness. In the absence of crystallization, an increase in the spinning velocity at constant T_d is accompanied by some increase in the deformation rate and a strong reduction of the cooling rate and viscosity gradient:

$$\begin{aligned} W &= 1/4\,\rho\pi d_L^2 V_L \\ T_d &= \text{const} \Rightarrow W \propto V_L \\ \left|\frac{-d\ln(\overline{T}-T_\infty)}{dz}\right| &\propto \frac{1}{\overline{V}^{2/3}} \\ \frac{d\eta}{dz} &= \frac{\partial\eta}{\partial\overline{T}}\frac{d\overline{T}}{dz} \propto \frac{1}{\overline{V}^{2/3}(\overline{T}-T_\infty)} \end{aligned} \tag{17}$$

The shape of the $V_L(F_0)$ function in Figure 3 is different from that for the regime of constant W.

In the range of low velocities, the initial force increases with increasing velocity, passes through a broad maximum, and then decreases. In the absence of crystallization, such behavior, resulting from competition between the deformation-rate and cooling effects, extends over the entire range of the variables. As in Figure 2, the $V_L(F_0)$ characteristic for crystallizing polymers involves two branches. The left-hand branch (dashed line) corresponds to the formation of amorphous fibers. The right-hand branch (solid line) appears only when crystalline fibers are formed.

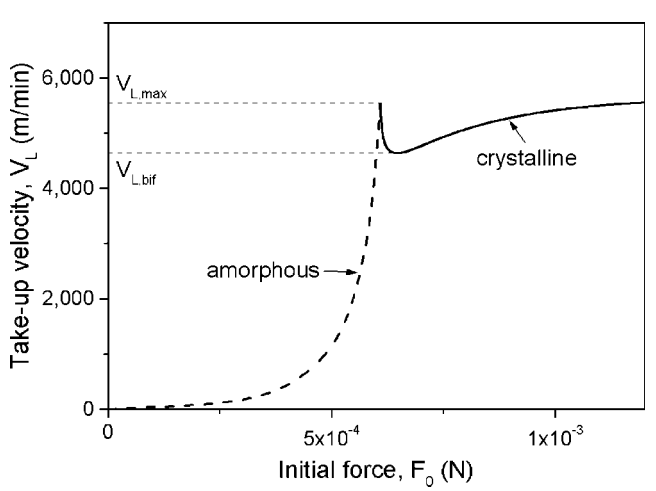

Figure 2 V_L versus F_0 calculated for the melt spinning of PET. W was constant (0.04 g/s). The standard set of material characteristics was used (Table I).

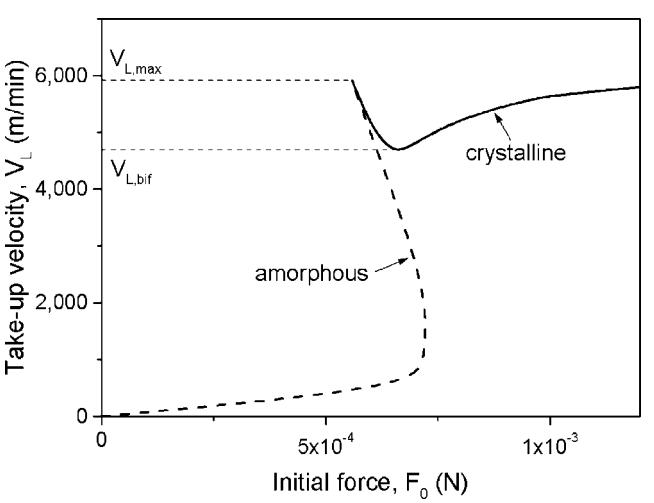

Figure 3 V_L versus F_0 calculated for the melt spinning of PET T_d was constant (5 dtex). The standard set of material characteristics was used (Table I).

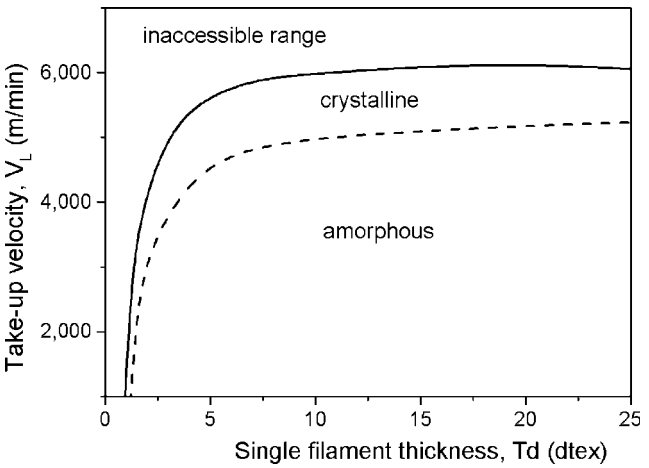

Figure 4 Different regions in the space of the spinning variables for PET. The standard set of material characteristics was used (Table I). The dashed line indicates the bifurcation velocity and the onset of crystallization, and the solid line indicates the maximum take-up velocity.

ACCESSIBLE AND INACCESSIBLE REGIONS IN THE SPACE OF SPINNING CONDITIONS

Using the model described in the previous sections, we calculated critical velocities $V_{L,\mathrm{bif}}$ and $V_{L,\mathrm{max}}$ for various spinning conditions. The resulting values show three regions in the space of the basic spinning variables ($V_L \times T_d$; Fig. 4).

In the range of low velocities and not too small filament thicknesses, amorphous fibers are obtained. Partially crystalline fibers appear in the intermediate range between the bifurcation- and maximum-velocity lines: $V_{L,\mathrm{bif}} < V_L < V_{L,\mathrm{max}}$. The region located above the solid line, $V_L > V_{L,\mathrm{max}}$, is inaccessible. Both the velocity at the onset of crystallization (dashed line) and the maximum take-up velocity (solid line) increase with increasing filament thickness, tending to level off at $T_d > 15$ dtex. For spinning very fine filaments ($T_d < 1$ dtex), only small speeds are available. The existing experimental evidence is generally consistent with such behavior.[31–34]

Figure 5 presents bifurcation and maximum take-up velocities calculated for 5-dtex PET fibers with three different molecular weights. A standard set of characteristics (Table I) is assumed. With the stress-crystallization parameter adjusted to the value of $A = 800$, the calculated lines are reasonably consistent with the experimental points.[32]

Detailed positions of the amorphous, crystalline, and inaccessible regions depend on material properties and spinning conditions. The simplified character of the model and uncertainty about some material characteristics do not guarantee reliable quantitative predictions. What can be obtained is a semiquantitative estimation of the effects of various material properties and process conditions on the dynamics of spinning and the structure of the resulting fibers. Such results may be useful in the optimization of existing processes and in the design of new spinning processes.

MAJOR FACTORS CONTROLLING ACCESSIBLE SPINNING CONDITIONS

There are two groups of factors that control the bifurcation of dynamic solutions and the limited range of spinning conditions. Stress-induced crystallization and crystallinity-dependent viscosity are primary conditions of bifurcation. If either or both effects are missing, no bifurcation will occur. The other group of factors (the molecular weight of the polymer and the thermal conditions of extrusion and cooling) may strongly affect bifurcation, provided that the primary conditions are satisfied. We will discuss these effects and discuss the possibility of their modification.

Stress-induced crystallization rate

A theoretical analysis of the bifurcation behavior[12] and our earlier simulations[9–11] have indicated the crucial role played by stress-induced crystallization. In our model, the effect of stress is described by parameter A in eq. (12). Few existing experimental data on PET[29] suggest A values in the range of 200–1000.

Figure 6 presents effect of parameter A on the spinning of PET fibers. In the case of purely thermal, stress-independent crystallization ($A = 0$), no bifurcation is predicted in a wide range of spinning conditions. Under such conditions, no maximum veloc-

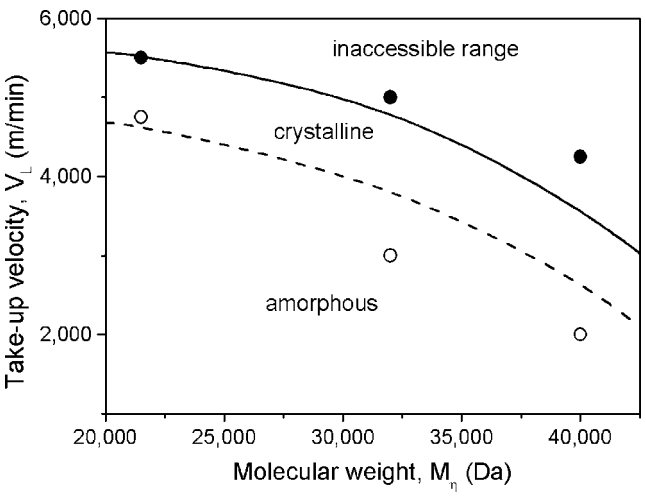

Figure 5 Bifurcation velocity and maximum take-up velocity for the spinning of 5-dtex PET filaments versus the average molecular weight. The lines indicate the numerical simulation, and the points indicate the experimental data of Huisman et al.[32]

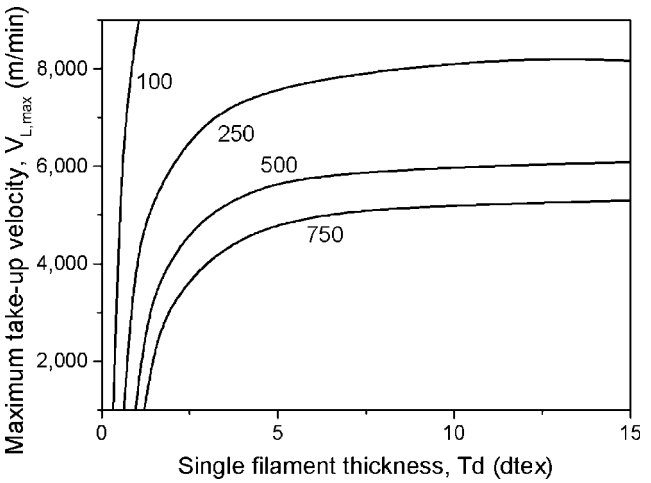

Figure 6 Maximum take-up velocity versus the filament titer calculated for PET fibers. The standard set of material characteristics was used (Table I). Parameter A [eq. (12)] is indicated.

ity can be defined. With increasing A values, the maximum take-up velocity is reduced, and the minimum filament thickness is increased. The desired expansion of the accessible range of spinning conditions, that is, an increase in the take-up velocity and/or a reduction of the minimum filament thickness, would require small values of parameter A. How can the reduction of A be realized?

An experimental and theoretical basis for empirical characteristic A is inadequate to suggest any chemical or physical changes. From a theoretical point of view, A is expected to be a temperature-dependent material characteristic related to the thermodynamic driving force for stress-induced crystallization.[35]

On the practical side, attempts were made to suppress molecular orientation and stress-induced crystallization in high-speed spinning of PET.[36–40] The method consists of using immiscible polymer additives (desirably liquid-crystalline), which take over subaffine internal stress in the polymer melt, reducing the molecular orientation and crystallization rate. The effects of such additives are similar to the reduction of parameter A and can be used for the appropriate modification of spinning PET and other crystallizable polymers.

Crystallinity-dependent viscosity

The other primary condition of bifurcation is the melt viscosity dependent on the degree of crystallinity. Our simulation was based on the concept of physical gelation,[16,22,30] leading to hyperbolic formula (10). It is assumed that small crystals that form in the undercooled polymer melt act as physical crosslinks. The result of such crosslinking is the formation of molecular aggregates, and when the critical crystallinity is reached, the fluid melt is converted into a solid gel.

A rough estimate of X_{cr} is based on the theory of crosslinking. According to Flory,[41] the gelation point is reached when the concentration of crosslinks approaches two crosslinks per primary polymer chain. Consider a polymer melt composed of n_{ch} chains with a primary (uncrosslinked) degree of polymerization, N_0. The molecular volume of a single monomer unit is v_0. Crystallization introduces n_X physical crosslinks, each with volume v_X. If we neglect the volume changes in the crystallization, these variables can be combined to yield the crystal-

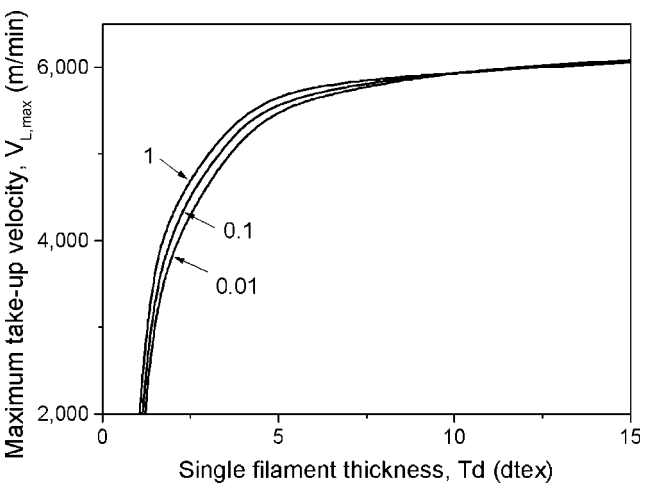

Figure 7 Maximum take-up velocity versus the filament titer calculated for PET fibers. The standard set of material characteristics was used (Table I). X_{cr} [eq. (10)] is indicated.

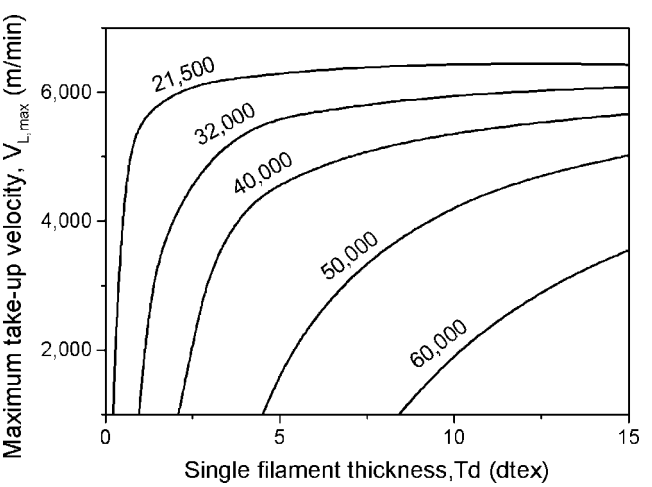

Figure 8 Maximum take-up velocity versus the filament titer calculated for PET fibers. The material characteristics from Tables I and II were used. M_η (Da) is indicated.

TABLE II
Molecular Weight of PET and Its Viscosity Characteristics

M_η (10^3 Da)	21.5	32	40	50	60
Intrinsic viscosity (dL/g)[a]	0.478	0.618	0.714	0.825	0.929
Melt viscosity parameter (kPa s)[b]	0.1948	0.7612	1.635	3.513	6.562
Activation energy (K)[c]	6923.7	6923.7	6923.7	6923.7	6923.7

[a] Reference 15.
[b] Reference 14.
[c] Reference 14.

linity, that is, the volume fraction of the crystalline phase, X:

$$X = \frac{n_X \cdot v_X}{n_{\mathrm{ch}} N_0 \cdot v_0} \tag{18}$$

The expression in the numerator represents the volume of the crystalline phase, and that in the denominator represents the total volume of the system. The number of crystallites (i.e., crosslinks) per primary chain and X_{cr} read as follows:[30]

$$\begin{aligned} \frac{n_X}{n_{\mathrm{ch}}} &= X \frac{N_0 \cdot v_0}{v_X} \\ \frac{n_X}{n_{\mathrm{ch}}} = 2 \Rightarrow X_{\mathrm{cr}} &= \frac{2_{v_X}}{N_0 \cdot v_0} \end{aligned} \tag{19}$$

It is evident that X_{cr} is inversely proportional to the degree of polymerization (or molecular weight) of the polymer. N_0 for typical fiber-forming polymers ranges from 200 (PET) to 4000 (PP). The number of monomer units in an effective crosslink (crystallite and crystal nucleus) is not known but should not exceed 5–50. Consequently, the critical crystallinity may be as small as 1% or several percent. Experiments of Floudas et al.[23] indicated a sharp upturn of the melt viscosity at a crystallinity in the range of 0.005–0.30, depending on the shear stress. In our simulations, the critical crystallinity required for gelation was rather arbitrarily assumed to be $X_{\mathrm{cr}} = 0.1$.

Figure 7 presents the effect of X_{cr} on the spinning of PET fibers (cf. Table I). Surprisingly, the results presented in Figure 7 show that the maximum take-up velocity and minimum filament thickness are insensitive to X_{cr} in the range of 0.01–1. Whenever hyperbolic (gelation-type) behavior is assumed, the space of the spinning variables splits into accessible and inaccessible regions, but the crystallinity level at which the critical conditions occur is not important. More theoretical and experimental research is needed before any conclusions leading to practical applications are drawn.

Molecular weight

The molecular weight is one of the secondary characteristics that affect bifurcation behavior, provided that the primary conditions (stress-induced crystallization and crystallinity-dependent viscosity) are satisfied. The most important effect of the molecular weight is the melt viscosity. It has been observed that fibers spun from PET with a higher molecular weight start to crystallize at lower spinning speeds, and the maximum take-up velocity is shifted to lower values.[31–34]

Figure 8 presents the effect of M_η on the melt spinning of PET fibers (for the characteristics, see Tables I and II). Three polymers are compared. The maximum take-up velocity and bifurcation velocity (the latter not indicated in the figure), are shifted to lower values; the more this happens, the higher M_η and the melt viscosity are. Similarly, with increasing molecular weight, the minimum filament thickness increases. Evidently, the melt spinning of ultrafine filaments is favored by the application of low-molecular-weight polymers. On the other hand, the molecular weight plays an important role in the development of the mechanical properties of fibers, and in every case, a reasonable compromise should be reached.

Cooling conditions

The temperature field around the spin line strongly affects the dynamics of melt spinning and the structural and mechanical characteristics of the resulting fibers. The simulations discussed previously are based on a simple spinning setup (Fig. 1) in which

TABLE III
Characteristics of Regular and Hot-Tube Spinning

	Hot-tube spinning		
Parameter	Upper cooling zone	Hot tube	Lower cooling zone
Length (m)	1.0	1.0	1.0
Temperature (°C)	20	100–210	20
Air blow speed (m/s)	0.4	0.0	0.0

	Regular spinning	
Parameter	Upper zone	Lower zone
Length (m)	1.0	2.0
Temperature (°C)	20	20
Air blow speed (m/s)	0.4	0.0

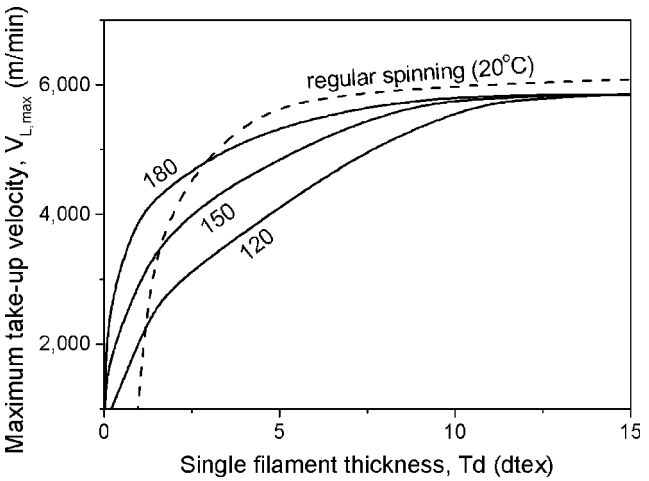

Figure 9 Maximum take-up velocity versus the filament titer calculated for PET fibers. The standard set of material characteristics was used (Table I). The solid lines indicate hot-tube spinning, and the dashed line indicates regular spinning (cf. Table III). T_{tube} (°C) is indicated.

the spin line is cooled by a transverse air stream with a constant temperature and a constant blow rate (see Table III). The modification of the temperature of the ambient air provides an important tool for affecting the melt-spinning process.

One of the suggested spinning systems consists of passing the spin line consecutively through three thermal zones:

- Cooling at room temperature (close to the spinneret).
- Heating in a tube.
- Cooling at room temperature (before winding).

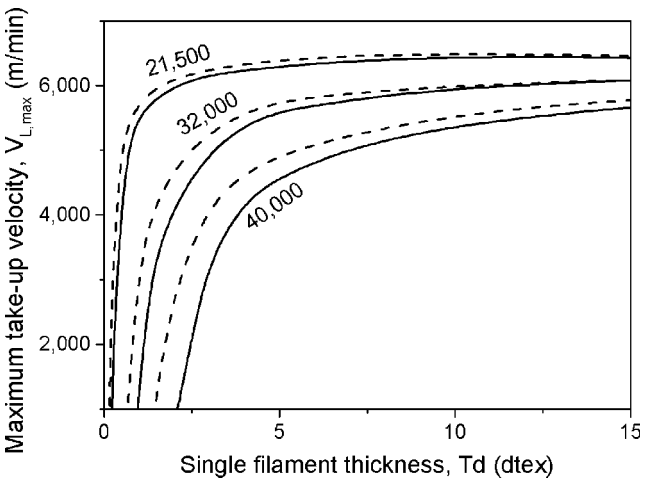

Figure 10 Maximum take-up velocity versus the filament titer calculated for PET fibers. The standard set of material characteristics was used (Table I). The solid lines indicate an extrusion temperature of $T_0 = 557$ K, and the dashed lines indicate $T_0 = 577$ K. The molecular weights (Da) are indicated (cf. Table IV).

TABLE IV
PET Melt Viscosity at the Extrusion Temperature

M_η (Da)	21,500	32,000	40,000
Melt viscosity at $T_0 = 284$°C (Pa s)	48.8	190.5	409.3
Melt viscosity at $T_0 = 304$°C (Pa s)	31.7	123.8	266.0

This hot-tube spinning system has been described in many patents and a few articles.[42–45] The dynamics of the process and structural development in the hot-tube spinning of PET fibers are described in refs. 10 and 46.

Consider a model hot-tube system described in Table III. Solidification in the upper cooling zone is followed by reheating within the tube and final cooling in the lower zone, before the filament is collected.

Figure 9 presents the effect of the tube temperature, T_{tube}, on the critical spinning conditions. An increase in T_{tube} leads to an increase in the maximum take-up velocity. In the range of thick filaments (above $T_d = 15$ dtex) the $V_{L,\max}$–T_d curves level off. Comparing hot-tube spinning (solid lines) with regular spinning (dashed line), we can observe that the latter admits lower speeds than the hot-tube setup in the range of $T_d < 1$ dtex and higher speeds for $T_d > 3$ dtex. In the intermediate range of the filament thickness, the characteristics $V_{L,\max}$ and T_d intersect each other. Thus, hot-tube spinning might offer an interesting solution for spinning thin filaments.

Extrusion temperature

The accessible range of spinning conditions can also be affected by the extrusion temperature and the viscosity of the melt in the vicinity of the spinneret. Shimizu et al.[19] observed significant effects of the extrusion temperature on the melt spinning of polypropylene fibers.

Figure 10 presents the maximum spinning velocities for two extrusion temperatures: $T_0 = 557$ and $T_0 = 577$ K (Table IV). An increase in T_0 moves the maximum take-up velocity to higher values and reduces the minimum filament thickness. The effect is rather weak for low-molecular-weight (and low-viscosity) melts. For spinning very high molecular weight polymers, the variation of T_0 offers another possibility for process modification.

DISCUSSION

The numerical simulation of the steady-state melt spinning of crystallizable polymers shows, under

some conditions, bifurcation of the dynamic solutions (Figs. 2 and 3). The same material properties and the same external conditions determine different dynamic characteristics: stress, velocity, and temperature profiles and different molecular orientation and crystallinity of the resulting fibers. Bifurcation seems to be controlled by stress-induced crystallization of the polymer coupled with crystallinity-dependent melt viscosity. In the space of basic spinning conditions (take-up velocity $\times$ filament thickness), two critical lines can be defined (Fig. 4). $V_{L,\mathrm{bif}}$ determines the bifurcation conditions and the onset of crystallization. The other line, $V_{L,\mathrm{max}}$, determines the maximum accessible take-up velocity. The space of the spinning conditions splits into three regions. The low-velocity region, $V_L < V_{L,\mathrm{bif}}$, corresponds to the formation of amorphous fibers; in the intermediate region, $V_{L,\mathrm{bif}} < V_L < V_{L,\mathrm{max}}$, partially crystalline fibers are obtained; and the region of velocities higher than $V_{L,\mathrm{max}}$ is inaccessible to melt spinning.

Detailed calculations have been performed for spinning PET. The results of the numerical simulation are qualitatively consistent with the experimental evidence.[5,32–34] Major factors affecting the bifurcation and maximum take-up velocity have been analyzed and discussed in various ways to expand the range of accessible spinning conditions (increasing the maximum spinning speed and reducing the minimum filament thickness). Two special spinning systems have also been analyzed: high-speed spinning with immiscible polymer additives suppressing stress-induced crystallization[36–40] and hot-tube spinning[42–46] modifying the temperature field and increasing the deformability of the spin line.

References

1. Ziabicki, A. Fundamentals of Fibre Formation; Wiley: London, 1976.
2. (a) Pearson, J. R. A.; Matovich, M. A. Ind Eng Chem Fundam 1969, 8, 605; (b) Pearson, J. R. A.; Shah, Y. T. Ind Eng Chem Fundam 1976, 13, 134.
3. (a) Petrie, C. J. S.; Denn, M. M. AIChE J 1976, 22, 209; (b) Petrie, C. J. S. Elongational Flows; Pittman: London, 1979.
4. Hyun, J. C. AIChE J 1978, 24, 418.
5. Kase, S. In High Speed Fiber Spinning; Ziabicki, A.; Kawai, H., Eds.; Interscience: New York, 1985; p 67.
6. Hyun, J. C. AIChE J 1978, 24, 426.
7. Lee, J. S.; Shin, D. M.; Jung, H. W.; Hyun, J. C. J Non-Newtonian Fluid Mech 2005, 130, 110.
8. Shin, D. M.; Lee, J. S.; Jung, H. W.; Hyun, J. C. Korea–Aust Rheol J 2005, 17, 63.
9. Ziabicki, A.; Jarecki, L.; Wasiak, A. Comput Theor Polym Sci 1998, 8, 143.
10. Jarecki, L.; Ziabicki, A.; Blim, A. Comput Theor Polym Sci 2000, 10, 63.
11. Jarecki, L.; Ziabicki, A. Polimery 2004, 49, 101.
12. Ziabicki, A.; Jarecki, L. Arch Mech 2006, 58, 4.
13. (a) Kase, S.; Matsuo, T. J Polym Sci Part A: Gen Pap 1965, 3, 2541; (b) Kase, S; Matsuo, T. J Appl Polym Sci 1968, 11, 251.
14. Dutta, A.; Nadkarni, V. M. Text Res J 1984, 54, 35.
15. Berkowitz, S. J Appl Polym Sci 1984, 29, 4353.
16. Ziabicki, A. J Non-Newtonian Fluid Mech 1988, 30, 157.
17. Krieger, I. M.; Dougherty, T. J. Trans Soc Rheol 1959, 3, 137.
18. Katayama, K.; Yoon, M. G. In High Speed Fiber Spinning; Ziabicki, A.; Kawai, H., Eds.; Interscience: New York, 1985; p 207.
19. Shimizu, J.; Okui, N.; Kikutani, T. In High Speed Fiber Spinning; Ziabicki, A.; Kawai, H., Eds.; Interscience: New York, 1985; p 429.
20. Titomanlio, G.; Speranza, V.; Brucato, V. Int Polym Proc J 1997, 12, 45.
21. Pantami, R.; Speranza, V.; Titomanlio, G. Int Polym Proc J 2001, 16, 61.
22. Lin, Y. G.; Mallin, D. T.; Chien, J. C. W.; Winter, H. H. Macromolecules 1991, 24, 850.
23. Floudas, G.; Hilliou, L.; Lellinger, D.; Alig, I. Macromolecules 2000, 33, 6466.
24. Tanner, R. I. Presented at the Hellenic Society of Rheology Conference, Patras, Greece, June 11, 2001.
25. (a) Ziabicki, A. Appl Polym Symp 1967, 6, 1; (b) Ziabicki, A Colloid Polym Sci 1996, 274, 209.
26. (a) Nakamura, K.; Watanabe, T.; Katayama, K.; Amano, T. J Appl Polym Sci 1972, 16, 1077; (b) Nakamura, K.; Watanabe, T.; Katayama, K.; Amano, T. 1973, 17, 1031.
27. Matsui, M. In High Speed Fiber Spinning; Ziabicki, A.; Kawai, H., Eds.; Interscience: New York, 1985; p 137.
28. Dumbleton, J. H. J Polym Sci Part A; Gen Pap 1968, 6, 798.
29. Alfonso, G. C.; Verdona, M. P.; Wasiak, A. Polymer 1978, 19, 711.
30. Ziabicki, A.; Jarecki, L.; Sorrentino, A. e-Polymers 2004, No. 072.
31. Dumbleton, J. H. Text Res J 1970, 40, 1035.
32. Huisman, R.; Heuvel, H. M.; van den Heuvel, C. J. M. Indian J Fibre Text Res 1991, 16, 7.
33. Heuvel, H. M.; Huisman, R. In High Speed Fiber Spinning; Ziabicki, A.; Kawai, H., Eds.; Interscience: New York, 1985; p 295.
34. Perez, G. In High Speed Fiber Spinning; Ziabicki, A.; Kawai, H., Eds.; Interscience: New York, 1985; p 333.
35. Ziabicki, A. Polimery 1973, 18, 615.
36. (a) Brody, H. J Appl Polym Sci 1986, 31, 2753; (b) Brody, H. Eur. Pat. 154,425 (1985).
37. Miles, I. S. J Appl Polym Sci 1987, 34, 2793.
38. Perez, G.; Jung, E. Proceedings of the International Fiber Science & Technology Conference, Hakone, Japan, 1985; p 64.
39. Brody, H. Proceedings of the International Fiber Science & Technology Conference, Hakone, Japan, 1985; p 230.
40. Sajkiewicz, P. American Textiles International – Fiber World, 11/1990; p FW2.
41. Flory, P. J. Principles of Polymer Chemistry; Cornell University Press: Ithaca, NY, 1953.
42. Cuculo, J. A.; Tucker, P. A.; Chen, G. Y.; Lin, C. Y.; Denton, J. Int Polym Process 1989, 4, 85.
43. Cuculo, J. A.; et al. U.S. Pat. 4,909,976 (1990).
44. Wang, H. H.; Hu, Y. J. Text Res J 1997, 67, 428.
45. Hayashi, S.; Katsuya, T.; Ishihara, H.; Yasuda, H. Sen-I Gakkaishi 1992, 48, 541.
46. Blim, A.; Ołdak, E.; Wasiak, A.; Jarecki, L. Polimery 2005, 50, 49.
47. Brandrup, J.; Immergut, E. H. Polymer Handbook; Interscience: New York, 1967.